Quantum-metric-enabled exciton condensate in double twisted bilayer graphene

Xiang Hu, Timo Hyart, Dmitry I. Pikulin, and Enrico Rossi

Phys. Rev. B **105**, L140506 — Published 18 April 2022

DOI: 10.1103/PhysRevB.105.L140506

Quantum-metric-enabled exciton condensate in double twisted bilayer graphene

Xiang Hu,[1] Timo Hyart,[2,3] Dmitry I. Pikulin,[4,5] and Enrico Rossi[1]

[1]*Department of Physics, William & Mary, Williamsburg, VA 23187, USA*
[2]*International Research Centre MagTop, Institute of Physics, Polish Academy of Sciences, Aleja Lotnikow 32/46, PL-02668 Warsaw, Poland*
[3]*Department of Applied Physics, Aalto University, 00076 Aalto, Espoo, Finland*
[4]*Microsoft Quantum, Redmond, Washington 98052, USA*
[5]*Microsoft Quantum, Station Q, Santa Barbara, California 93106-6105, USA*

(Dated: March 29, 2022)

Flat-band systems are a promising platform for realizing exotic collective ground states with spontaneously broken symmetry because the electron-electron interactions dominate over the kinetic energy. A collective ground state of particular interest is the chased after exciton condensate (EC). However, in flat band systems other collective ground states can compete with an EC phase, and the conventional treatment of the effect of thermal and quantum fluctuations predicts the EC phase should be unstable. Here, using double twisted bilayer graphene (TBLG) heterostructures as an example, we show that for realistic interaction strengths the EC phase is favored with respect to other TBLG's phases – orbital magnetism and superconductivity– when the TBLGs have opposite doping, and that the quantum metric of the Bloch wave functions stabilizes the EC, reversing the conclusion that would be drawn from the conventional approach in which quantum metric contributions are neglected. Our results suggest that the quantum metric plays a critical role in determining the stability of exciton condensates in double layers formed by systems with flat-bands.

An exciton is a bosonic quasiparticle formed by an electron (e) bound to a hole (h). A large number of excitons can become phase coherent and form a collective state known as exciton condensate (EC) [1, 2]. Already in the mid 70's it was proposed [3, 4] that spatially separating electrons and holes should facilitate the formation of a thermodynamically stable EC. Such separation can be realized in e-h semiconductor double layers, in which a thin dielectric separates the layers and distinct metal gates are used to create an excess density of electrons in one layer which equals the excess density of holes in the other one. Great advances in the fabrication of heterostructures made possible the realization of several novel double layers in which ECs could be realized [5–24]. It was proposed that ECs could be formed in graphene double layers [5, 6], but experimentally no strong signatures have been observed, so far. It was then proposed that ECs could be realized in systems based on double bilayer graphene (BLG) [8, 9, 16], given that at low energies BLG's bands are qualitatively flatter than graphene's, and recent experiments show signatures that are consistent with the formation of an EC [18]. These results, combined with the ones for quantum Hall (QH) bilayers [25–30], in which the kinetic term of each layer is completely quenched, would suggest that, in general, the formation of an EC is favored in bilayers formed by 2D systems with flat bands. As a consequence, double twisted bilayer graphene (TBLG), in which the bands can be made extremely flat by tuning the twist angle θ between graphene sheets [31–38] appears to be an ideal system to seek the realization of ECs without external magnetic fields. This expectation, however, is in part naive. First, the flatness of the bands is associated with strong screening of the interlayer Coulomb interaction that is the driver of the EC instability. This obstacle can be overcome by tuning the system into the strong coupling regime, where the e-(h-)densities are sufficiently small so that the coherence length ξ of the EC is smaller than the average distance between particles [10]. Second, the stiffness (ρ_s) of the EC, i.e. its robustness against thermal and quantum fluctuations, is conventionally expected to decrease as the bands become flatter and ultimately vanish in the limit of perfectly flat bands.

In this work we show that the second obstacle in general might not be present if one considers the contribution to ρ_s due to the quantum metric of the eigenstates of the EC. We consider the specific case of double layers formed by an e-doped TBLG and a h-doped TBLG separated by a thin insulating barrier [Fig. 1(a)]. We first perform a mean field calculation, in which the order parameters for the EC, superconductivity (SC) and orbital magnetism (OM) are treated on equal footing, to identify the regions of the the phase diagram as a function of dopings in the upper (U) and lower (L) TBLG where the EC is favored. We then calculate ρ_s for the EC and show that the contribution to it due to the quantum metric is essential to make it positive and therefore to stabilize the EC. In addition, we describe how ρ_s depends on the twist angle and find that the most favorable twist angle θ to realize a stable EC is not the magic angle. We also obtain the Berezinskii-Kosterlitz-Thouless (BKT) temperature $T_{\rm BKT}$ [39, 40] as function of θ. Considering that most systems with almost flat bands are multiband systems, our results have universal relevance for the understanding of the conditions necessary to realize ECs: they show that to realize an EC in 2D bilayers the flatness of the bands of the layers must be accompanied by a significant quantum metric contribution to the EC's stiffness. Our results also allow to understand in a new light the conditions that make possible the realization and observation of ECs in QH bilayers [41, 42].

The double TBLG system is described by the Hamiltonian $\hat{H} = \hat{H}^U + \hat{H}^L + \hat{H}_{\rm int}$ where $\hat{H}^{U/L}$ is the single-particle Hamiltonian for the U/L TBLG and $H_{\rm int}$ describes the e-e interactions. We assume θ to be the same for the two

TBLGs. For small θ the low energy states of a TBLG are well described by an effective tight-binding Hamiltonian *in momentum space* with the lattice sites $\{\mathbf{b} = m_1\mathbf{b}_1 + m_2\mathbf{b}_2\}$ corresponding to the reciprocal lattice vectors of the moiré lattice. The on-site Hamiltonians describe the Dirac points of graphene with Fermi velocity $v_F = 10^6$ m/s, and the nearest-neighbor hopping matrices T_i describe the coupling between the layers with tunneling strength $w = 118$ meV [33, 43–45]. Here $\mathbf{b}_1 = (\sqrt{3}Q, 0), \mathbf{b}_2 = (\sqrt{3}Q/2, 3Q/2)$, $m_1, m_2 \in \mathbb{Z}$, $Q = (8\pi/3a_0)\sin(\theta/2)$ and a_0 is the lattice constant of graphene. Recent experimental and theoretical results suggest that for a single TBLG the strongest instabilities are orbital-magnetism (OM), characterized by a finite polarization in sublattice space, and superconductivity (SC) [46–48]. We therefore decouple the interactions within the same TBLG via the mean fields $\Delta^{\rm OM,SC}_{\mathbf{b}l\sigma l'\sigma'}(l = l', \sigma = \sigma')$, where the indices l, l' (σ, σ') correspond to the layer (sublattice) degrees of freedom freedom within the U or L TBLG [43]. The interaction between electrons in different TBLGs is decoupled via the EC mean field $\Delta^{\rm EC}_{\mathbf{b}l\sigma l'\sigma'}$. We assume the EC, SM, and OM phases obey the spin-rotation symmetry. Given the flatness of TBLG's low energy bands, in the mean-field approximation all the interactions can be replaced by effective *local* interactions [43]. We denote the strengths of the effective local interaction in the OM, SC and EC channels as $V_{\rm OM}$, $V_{\rm SC}$ and $V_{\rm EC}$, respectively. We expect $V_{\rm OM} > V_{\rm SC} \sim V_{\rm EC}$, but it is challenging to estimate the precise values of the interaction strengths because of the interplay of screening effects and collective instabilities. Thus, we adopt a pragmatic approach: we set $V_{\rm OM} = 130$ meV·nm^2, and $V_{\rm SC} = 75$ meV·nm^2 so that the corresponding critical temperatures $T_c^{\rm OM}$ and $T_c^{\rm SC}$ are in good agreement with the experimental observations [34, 37], and consider different range of values for $V_{\rm EC}$, $60 - 100$ meV·nm^2, for which $T_c^{\rm EC} \sim 1 - 4$ K, and the system is in a strong coupling regime where the screening does not prevent the formation of the EC.

The gap equations for each order parameter (OP) $\Delta^{\rm OP}_{\bar\alpha}$, where OP $= \{{\rm OM}, {\rm SC}, {\rm EC}\}$, and $\bar\alpha$ is a collective index, can be linearized close to the critical temperature $T_c^{\rm OP}$: $\Delta^{\rm OP}_{\bar\alpha} = \sum_{\bar\beta} \chi^{\rm OP}_{\bar\alpha\bar\beta}\Delta^{\rm OP}_{\bar\beta}$, where $\chi^{\rm OP}_{\bar\alpha\bar\beta}$ is the bare susceptibility, independent of $\Delta^{\rm OP}_{\bar\alpha}$. $T_c^{\rm OP}$ is obtained as the temperature T for which the largest eigenvalue of $\chi^{\rm OP}_{\bar\alpha\bar\beta}$ is equal to 1. The expressions of $\chi^{\rm OP}_{\bar\alpha\bar\beta}$ for each phase are given in [43]. In Fig. 1(b) we show the phase diagram, as function of doping in each TBLG, for $V_{\rm EC} = 60$ meV·nm^2, obtained by identifying the highest $T_c^{\rm OP}$. We have verified for several (μ_U, μ_L) value pairs that the results obtained from the linearized and non-linearized gap equations are consistent. Close to $\nu_U = \nu_L = 0$ the correlated insulating phase OM is favored, whereas introducing equal electron densities in the two TBLGs $\mu_L \sim \mu_U$ favors the SC phase [49]. When the excess density of electrons in one TBLG equals the excess density of holes in the other TBLG, $\mu_U \sim -\mu_L$, the EC becomes dominant. In our system the EC is formed by states in physically different TBLGs, no pairing between states in bands with opposite Chern number is assumed, and so the topology of the low energy bands does not penalize the formation of a uniform *inter-TBLG* EC state [50].

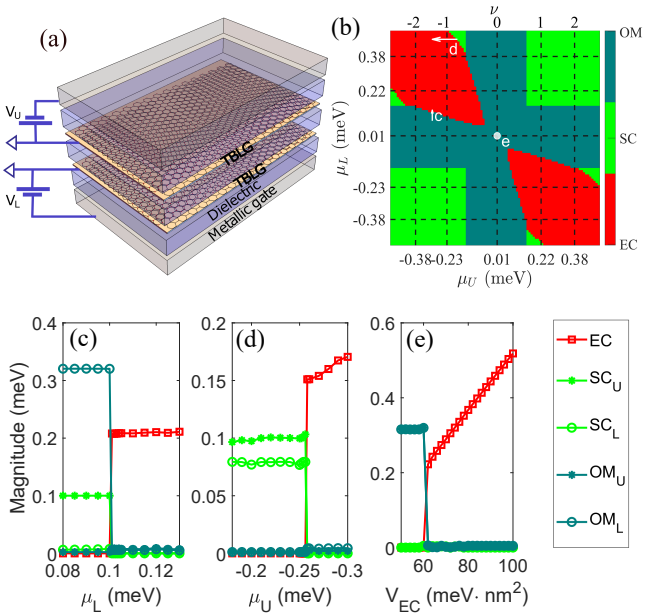

FIG. 1. (a) Proposed experimental setup. (b) Phase diagram of double-TBLG as a function of μ_U and μ_L for $\theta = 1.00°$. (c,d) Phase transitions as a function of dopings along the arrows shown in (b). (e) Phase transition as a function of $V_{\rm EC}$ at $\nu_U = \nu_L = 0$. The legend ${\rm SC(OM)_{U(L)}}$ represents the SC (OM) phase in the Upper (Lower) TBLG.

To investigate the possible coexistence of ordered phases [51] we have solved across several phase boundaries the full non-linear gap equations in which all the order parameters are allowed to be nonzero. We used large numbers of random initial conditions and identified the solution with the smallest total energy as the ground state. Fig. 1 (c) and (d) show the evolution of the order parameters across the OM/EC and SC/EC phase boundaries, respectively. In both cases the results suggest that the system undergoes a first-order quantum phase transition as the dopings are varied in Fig. 1(b). Fig. 1(e) shows the evolution of the order parameters as a function of $V_{\rm EC}$ at the neutrality point. Also in this case the transition appears to be first order. Figure 1(e) suggest that for $V_{\rm EC} > 60$ mev·nm^2 the EC is favored in a significant region of the (μ_U, μ_L) plane. In the reminder we focus on the $\mu_L = -\mu_U \equiv \mu$ regime, with μ sufficiently large, and set $V_{\rm EC} = 100$ meV·nm^2 so that, at the mean-field level, the EC phase is dominant. To simplify the notation in the sections below the EC label is implied.

Fig. 2 shows how T_c scales with μ and θ close to the magic angle $\theta_M = 1.05°$. T_c is largest when $\theta = \theta_M$, twist angle for which the bands are flattest, and decreases quickly when θ is tuned away from θ_M. The solution of the gap equation reveals that $\Delta_{\mathbf{b}l\sigma l'\sigma'}$ has several non-zero components. We performed the singular value decomposition (SVD), $\Delta_{\mathbf{b}l\sigma l'\sigma'} = USV^\dagger$, where S is a diagonal matrix whose diagonal elements are the *singular values* of $\Delta_{\mathbf{b}l\sigma l'\sigma'}$. Fig. 3(a) shows that the largest 20

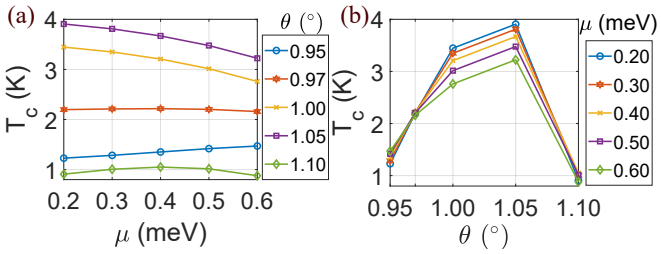

FIG. 2. (a) T_c as a function of $\mu = \mu_L = -\mu_U$ and different values of twist angle θ. (b) T_c as a function of θ and different values of μ.

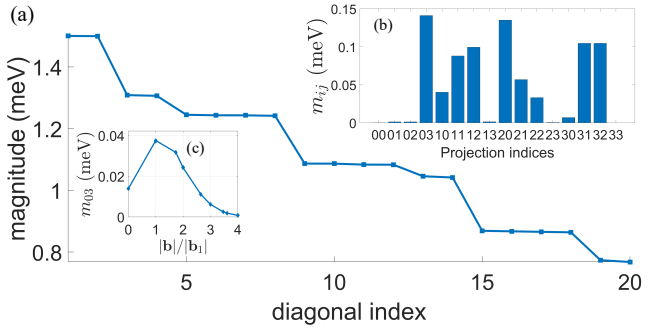

FIG. 3. (a) The first twenty singular values of the SVD decomposition $\Delta_{\mathbf{b}l\sigma l'\sigma'} = USV^\dagger$. (b) Amplitudes of the order parameter components m_{ij}. (c) Scaling with $|\mathbf{b}|$ of m_{03}. Here $\theta = 1.05°$ and $\mu = 0.30$ meV.

singular values (in total we have 484 singular values [43]) are of comparable size confirming the multi-component nature of the order parameter.

To better understand the orbital structure of $\Delta_{\mathbf{b}l\sigma l'\sigma'}$ we calculated its projections on the 4×4 matrices $\kappa_i \otimes \sigma_j$ as $m_{ij} = [\sum_{\mathbf{b}} \|a_{ij}^{(\mathbf{b})}\|^2]^{1/2}$, $a_{ij}^{(\mathbf{b})} = (1/4)\mathrm{Tr}[\Delta_{\mathbf{b}l\sigma l'\sigma'}\kappa_i \otimes \sigma_j]$, where κ_i (σ_i) are the Pauli matrices in the layer (sublattice) space. We see, Fig. 3 (b), that m_{03} is the largest projection, but several other projections are comparable to it. The fairly even distribution of the EC's order parameter over different orbital channels is paralleled by its fairly slow decay with $|\mathbf{b}|$, see Fig. 3(c). These results are consistent with the SVD's result that $\Delta_{\mathbf{b}l\sigma l'\sigma'}$ describes a multi-component order parameter. This is in contrast with the results for the case of superconducting pairing in isolated TBLG where the pairing is dominated by a single channel and the magnitude of the order parameter decreases quickly with $|\mathbf{b}|$ [48, 52].

Fig. 4 shows the low energy bands along the $\gamma-\kappa_+-\nu-\gamma-\bar{\nu}$ path in the moiré Brillouin zone (BZ) [43] for $\theta = 1.05°$, and $\theta = 1.00°$, in the presence of the EC condensate. For $\theta = 1.05°$ the very large Fermi velocity of the low energy bands at the γ point prevents the EC from opening a gap at this point. As θ is tuned away from θ_M the singularity at the γ point morphs into two very small e-h pockets, Fig. 4(b). The results of Fig. 4(a,b) show that in double layer TBLG the EC is expected to be, strictly speaking, gapless. However, given

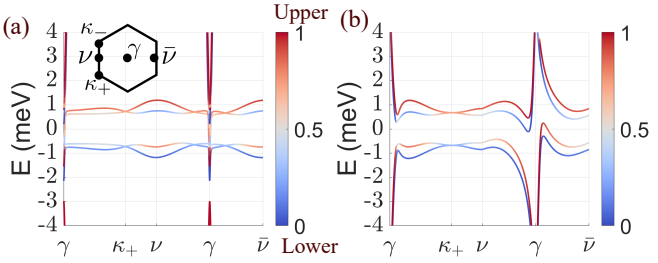

FIG. 4. Band structures in the EC phase at $T = 0$ and $\mu = 0.30$ meV for (a) $\theta = 1.05°$ and (b) $\theta = 1.00°$. The colorbar indicates how much the eigenstate is localized in the U/L TBLG. The inset in (a) shows the moiré Brillouin zone.

that the gapless nature is due to a very small number of states close to a single point of the BZ, the density of states is very negligible within the EC's gap (see [43]), and so we expect that the transition to the EC state could be clearly observed in transport and spectroscopy measurements.

We now consider the stability of the EC with respect to fluctuations. The dominant fluctuations are the ones of the phase, $\varphi(\mathbf{r})$, of the order parameter: $\Delta \to \Delta e^{i\varphi(\mathbf{r})}$. Expanding the action in the long-wavelength limit around the saddle point identified by the mean-field solution we have $S = \hat{S}_0 + \int d\tau \int d\mathbf{r} \frac{1}{2}\rho^s_{\alpha\beta}\partial_{r_\alpha}\varphi\partial_{r_\beta}\varphi$, where S_0 is the action at the saddle point, and $\rho^s_{\alpha\beta}$ is the $\alpha\beta$ component of the EC's stiffness. The EC is stable when $\rho^s_{\alpha\beta}$ is positive-definite. For a multiband system $\rho^s_{\alpha\beta}$ is given by the general expression [53, 54]:

$$\rho^s_{\alpha\beta} = \sum_{\mathbf{k},i,j} \frac{n_F(E_j) - n_F(E_i)}{E_i - E_j} \left(\frac{1}{4A}\langle\psi_i|\hat{v}_\alpha|\psi_j\rangle\langle\psi_j|\hat{v}_\beta|\psi_i\rangle - \frac{1}{A}\langle\psi_i|\hat{v}_{cf,\alpha}|\psi_j\rangle\langle\psi_j|\hat{v}_{cf,\beta}|\psi_i\rangle \right), \quad (1)$$

where E_i ($|\psi_i\rangle$) are the eigenvalues (eigenstates) of the mean-field Hamiltonian H_{MF}, $n_F(E)$ is the Fermi-Dirac distribution, A is the area of the sample, $\hat{v}_\alpha(\mathbf{k}) = \partial H_{\mathrm{MF}}/\partial k_\alpha$ and $\hat{v}_{cf,\alpha}(\mathbf{k}) = (1/2)\gamma_z \partial H_{\mathrm{MF}}/\partial k_\alpha$ are the components of the regular and counterflow velocity operators, respectively, γ_z is the Pauli matrix acting in the U/L subspace, and $\mathbf{k} = (k_x, k_y)$ is the Bloch wave vector. In our case, $\rho^s_{xy} = \rho^s_{yx} = 0$, and $\rho^s_{xx} = \rho^s_{yy} \equiv \rho_s$. For a multi-band system we can identify a conventional contribution, to ρ_s, $\rho^{s,\mathrm{conv}}$, arising almost exclusively from intraband terms (*same band index in the electron or hole subspace*), and a "geometric" contribution, $\rho^{s,\mathrm{geom}}$, due to interband terms (*different band indexes in both the electron and hole subspaces*), and write $\rho^s = \rho^{s,\mathrm{conv}} + \rho^{s,\mathrm{geom}}$. Because $\rho^{s,\mathrm{geom}}$ is closely connected to the quantum metric of the Hilbert space spanned by the eigenstates of H_{MF} [52–57], it is often called a geometric contribution to the superfluid stiffness.

Fig 5 shows how $\rho^{s,\mathrm{conv}}$, $\rho^{s,\mathrm{geom}}$ and ρ^s depend on μ and θ. All the results were obtained for $\mathcal{T} = 20$ mK $\ll T_c$. We notice that ρ_s does not grow with μ contrary to the conventional

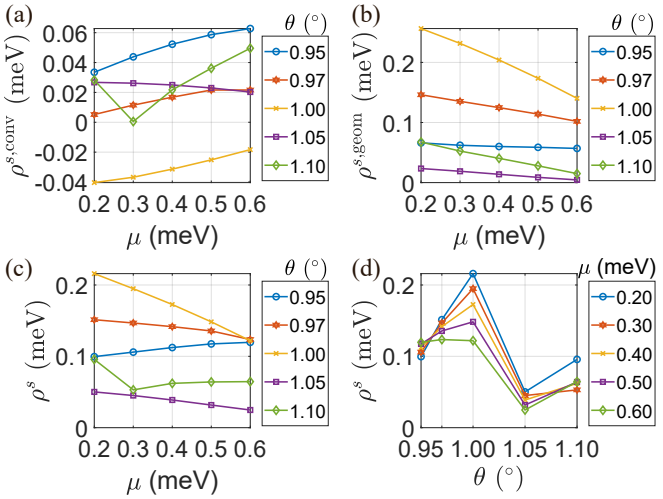

FIG. 5. (a) Conventional $\rho^{s,\mathrm{conv}}$, (b) geometric $\rho^{s,\mathrm{geom}}$, and (c) total stiffness ρ^{s} as a function of μ for different values of θ. (d) ρ^{s} vs. θ for different values of μ.

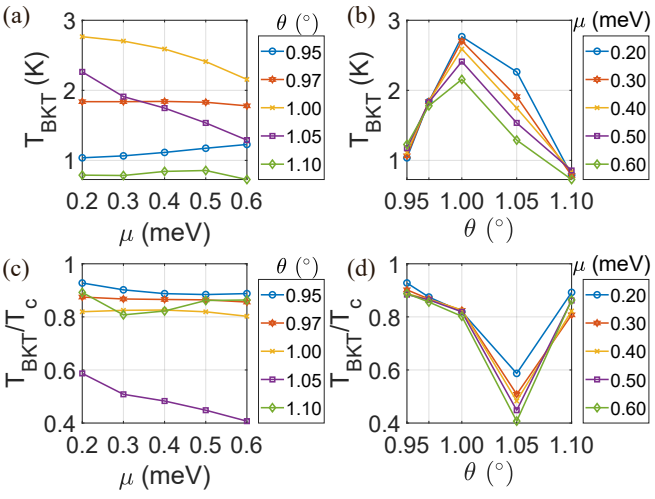

FIG. 6. (a) T_{BKT} as a function of μ for different values of θ. (b) T_{BKT} as a function of θ for different values of μ. (c), (d) T_{BKT}/T_c as a function of μ, θ, respectively.

result $\rho_s \propto \mu$. For $\theta = 1.05°$, and $\theta = 1.10°$, $\rho^{s,\mathrm{conv}}$ and $\rho^{s,\mathrm{geom}}$ are comparable and the relative weight changes with μ. For all the other twist angles considered $\rho^{s,\mathrm{geom}}$ is larger than $\rho^{s,\mathrm{conv}}$, regardless of μ.

The results of Fig. 2 (a) show that the mean field critical temperature T_c at $\theta = 1.00°$ is only slightly smaller than at $\theta = \theta_M$, and therefore that, at the mean-field level, double-layer TBLG with $\theta = 1.00°$ is a very good candidate for the realization of an EC. However, strikingly, for $\theta = 1.00°$ we find that $\rho^{s,\mathrm{conv}}$ for the EC is negative for all the values of μ, see Fig. 5 (a) (this can happen because of the lack of particle-hole symmetry). This result would lead us to conclude that for $\theta = 1.00°$ the EC is fragile against fluctuations and therefore not a stable ground state, despite the relatively large value of T_c. This conclusion is reversed if one takes into account the geometric contribution to ρ_s, Fig. 5 (b): for $\theta = 1.00°$ the $\rho^{s,\mathrm{geom}}$ is positive and much larger, in absolute value, than $\rho^{s,\mathrm{conv}}$, guaranteeing the robust stability of the EC. In fact, Figs. 5 (c), (d) allow us to conclude that the EC is most stable for $\theta = 1.00°$, not for $\theta = \theta_M$ as one would infer from the mean-field results.

The results of Fig. 5(c),(d) can be used to obtain T_{BKT}, via the equation $k_B T_{\mathrm{BKT}} = 2\pi\rho^{s}[\Delta(T_{\mathrm{BKT}}), T_{\mathrm{BKT}}]$, where we have taken into account the valley and spin degeneracies. For the dependence of Δ on $\mathcal{T}$ we can adopt the BCS scaling $\Delta(\mathcal{T}) = 1.764 k_B T_c (1 - \mathcal{T}/T_c)^{1/2}$, with k_B the Boltzmann's constant. The results for T_{BKT} are shown in Fig. 6. From Fig. 6 (a), (b) we see that, contrary to the mean-field results, the twist angle for which the critical temperature T_{BKT} is largest is not θ_M, but $\theta = 1.00°$, for all the values of μ. Indeed T_{BKT} at $\theta = 1.00°$ is up to 50% larger than at θ_M. This somewhat surprising result arises entirely from the geometric contribution to ρ_s. It is interesting to notice that, contrary to the conventional wisdom, for some twist angles T_{BKT} decreases, rather than increasing, with μ. Such behavior is particularly marked for $\theta = 1.00°$ and $\theta = \theta_M$, Fig. 6 (a), due to the significant decrease of the geometric contribution to ρ_s, as seen in Fig. 5. Figures 6 (c), (d) show how the ratio T_{BKT}/T_c scales with μ and θ, respectively. It is particularly interesting to see that, for all values of μ, T_{BKT}/T_c is minimum at θ_M.

In summary, we have studied the competition between OM, SC and EC phases as a function of the dopings of the layers via comprehensive mean-field calculations in double TBLG systems. We have discussed the nature of the phase transitions, and we have shown that for realistic interaction strengths the EC phase is favored when the TBLGs have sufficiently large and opposite dopings. We then studied the stiffness ρ_s of the EC and demonstrated that the quantum metric contribution to ρ_s is essential to make ρ_s positive so that the EC is stable against fluctuations. A "conventional" study of the EC's stability that does not include interbands terms would lead to the conclusion that in flat-band double layers ECs can be unstable. However, we found that this conclusion is reversed if the interband terms responsible for the quantum metric of the flat bands are taken into account. Finally, we obtained T_{BKT} for the ECs and found that the largest T_{BKT} is realized not at the magic angle, $\theta = 1.05°$, but at $\theta = 1.00°$. The results present a comprehensive and detailed picture of the possible correlated states of double-twisted bilayer graphene, and show the role played by the quantum metric on the stability and T_{BKT} of the exciton condensate in double-twisted bilayer graphene and so should constitute a useful guide to experimentalists studying the correlated phases of these novel systems. In a more general context, our findings point to the importance of the quantum metric for the understanding of the physics of ECs in flat band systems, including QH and moiré bilayers [58–60].

X.H and E.R. acknowledge support from ARO (Grant No.

W911NF-18-1-0290) and NSF (Grant No. DMR- 1455233). E.R. also thanks the Aspen Center for Physics, which is supported by NSF Grant No. PHY-1607611, and KITP, supported by Grant No. NSF PHY1748958, where part of this work was performed. X.H acknowledge the hospitality of Hunan Normal University. The authors acknowledge William & Mary Research Computing for providing computational resources. Part of the calculations were performed on the Extreme Science and Engineering Discovery Environment (XSEDE) [61] Stampede2 at TACC through allocation TG-PHY210052. The research was partially supported by the Foundation for Polish Science through the IRA Programme co-financed by EU within SG OP.

[1] L. V. Keldysh and Y. E. Kopaev, Possible instability of the semimetallic state toward Coulomb interaction, Sov. Phys. Solid State **6**, 2219 (1965).
[2] B. Halperin and T. Rice, The excitonic state at the semiconductor-semimetal transition (Academic Press, 1968) pp. 115 – 192.
[3] Y. E. Lozovik and V. I. Yudson, Feasibility of superfluidity of paired spatially separated electrons and holes - new superconductivity mechanism, Jetp Lett. **22**, 274 (1975).
[4] Y. E. Lozovik and V. I. Yudson, Novel mechanism of superconductivity - pairing of spatially separated electrons and holes, Zhurnal Eksperimentalnoi I Teoreticheskoi Fiziki **71**, 738 (1976).
[5] H. Min, R. Bistritzer, J.-J. Su, and A. H. MacDonald, Room-temperature superfluidity in graphene bilayers, Phys. Rev. B **78**, 121401(R) (2008).
[6] C. Zhang and Y. N. Joglekar, Excitonic condensation of massless fermions in graphene bilayers, Phys. Rev. B **77**, 233405 (2008).
[7] M. Y. Kharitonov and K. B. Efetov, Electron screening and excitonic condensation in double-layer graphene systems, Physical Review B **78**, 241401(R) (2008).
[8] J. Zhang and E. Rossi, Chiral superfluid states in hybrid graphene heterostructures, Phys. Rev. Lett. **111**, 086804 (2013).
[9] A. Perali, D. Neilson, and A. R. Hamilton, High-temperature superfluidity in double-bilayer graphene, Phys. Rev. Lett. **110**, 146803 (2013).
[10] D. Neilson, A. Perali, and A. R. Hamilton, Excitonic superfluidity and screening in electron-hole bilayer systems, Phys. Rev. B **89**, 060502(R) (2014).
[11] D. I. Pikulin and T. Hyart, Interplay of exciton condensation and the quantum spin hall effect in $InAs/GaSb$ bilayers, Phys. Rev. Lett. **112**, 176403 (2014).
[12] M. M. Fogler, L. V. Butov, and K. S. Novoselov, High-temperature superfluidity with indirect excitons in van der Waals heterostructures, Nature Communications **5**, 4555 (2014).
[13] D. I. Pikulin, P. G. Silvestrov, and T. Hyart, Confinement-deconfinement transition due to spontaneous symmetry breaking in quantum Hall bilayers, Nature Communications **7**, 10462 (2016).
[14] J. I. A. Li, T. Taniguchi, K. Watanabe, J. Hone, and C. R. Dean, Excitonic superfluid phase in double bilayer graphene, Nature Physics **13**, 751 (2017).
[15] B. Debnath, Y. Barlas, D. Wickramaratne, M. R. Neupane, and R. K. Lake, Exciton condensate in bilayer transition metal dichalcogenides: Strong coupling regime, Physical Review B **96**, 174504 (2017).
[16] J.-J. Su and A. H. MacDonald, Spatially indirect exciton condensate phases in double bilayer graphene, Phys. Rev. B **95**, 045416 (2017).
[17] L. Du, X. Li, W. Lou, G. Sullivan, K. Chang, J. Kono, and R.-R. Du, Evidence for a topological excitonic insulator in InAs/GaSb bilayers, Nature Communications **8**, 1971 (2017).
[18] G. W. Burg, N. Prasad, K. Kim, T. Taniguchi, K. Watanabe, A. H. MacDonald, L. F. Register, and E. Tutuc, Strongly enhanced tunneling at total charge neutrality in double-bilayer graphene-WSe_2 heterostructures, Phys. Rev. Lett. **120**, 177702 (2018).
[19] K. Tran, G. Moody, F. Wu, X. Lu, J. Choi, K. Kim, A. Rai, D. A. Sanchez, J. Quan, A. Singh, J. Embley, A. Zepeda, M. Campbell, T. Autry, T. Taniguchi, K. Watanabe, N. Lu, S. K. Banerjee, K. L. Silverman, S. Kim, E. Tutuc, L. Yang, A. H. MacDonald, and X. Li, Evidence for moiré excitons in van der Waals heterostructures, Nature **567**, 71 (2019).
[20] Z. Wang, D. A. Rhodes, K. Watanabe, T. Taniguchi, J. C. Hone, J. Shan, and K. F. Mak, Evidence of high-temperature exciton condensation in two-dimensional atomic double layers, Nature **574**, 76 (2019).
[21] X. Liu, Z. Hao, K. Watanabe, T. Taniguchi, B. I. Halperin, and P. Kim, Interlayer fractional quantum Hall effect in a coupled graphene double layer, Nature Physics **15**, 893 (2019).
[22] Y. H. Kwan, Y. Hu, S. H. Simon, and S. A. Parameswaran, Excitonic fractional quantum Hall hierarchy in moiré heterostructures, arXiv:2003.11559 (2020).
[23] Y. H. Kwan, Y. Hu, S. H. Simon, and S. A. Parameswaran, Exciton band topology in spontaneous quantum anomalous hall insulators: Applications to twisted bilayer graphene, Phys. Rev. Lett. **126**, 137601 (2021).
[24] Y. Shimazaki, I. Schwartz, K. Watanabe, T. Taniguchi, M. Kroner, and A. Imamolu, Strongly correlated electrons and hybrid excitons in a moiré heterostructure, Nature **580**, 472 (2020).
[25] I. B. Spielman, J. P. Eisenstein, L. N. Pfeiffer, and K. W. West, Resonantly Enhanced Tunneling in a Double Layer Quantum Hall Ferromagnet, Physical Review Letters **84**, 5808 (2000).
[26] A. Stern, S. M. Girvin, A. H. MacDonald, and N. Ma, Theory of interlayer tunneling in bilayer quantum hall ferromagnets, Phys. Rev. Lett. **86**, 1829 (2001).
[27] J. P. Eisenstein and A. H. MacDonald, BoseEinstein condensation of excitons in bilayer electron systems, Nature **432**, 691 (2004).
[28] E. Rossi, A. S. Núñez, and A. H. MacDonald, Interlayer Transport in Bilayer Quantum Hall Systems, Physical Review Letters **95**, 266804 (2005).
[29] A. D. K. Finck, J. P. Eisenstein, L. N. Pfeiffer, and K. W. West, Exciton Transport and Andreev Reflection in a Bilayer Quantum Hall System, Physical Review Letters **106**, 236807 (2011).
[30] T. Hyart and B. Rosenow, Quantitative description of Josephson-like tunneling in $\nu_T = 1$ quantum Hall bilayers, Physical Review B **83**, 155315 (2011).
[31] J. M. B. Lopes dos Santos, N. M. R. Peres, and A. H. Castro Neto, Graphene bilayer with a twist: Electronic structure, Phys. Rev. Lett. **99**, 256802 (2007).
[32] E. Suárez Morell, J. D. Correa, P. Vargas, M. Pacheco, and Z. Barticevic, Flat bands in slightly twisted bilayer graphene: Tight-binding calculations, Physical Review B **82**, 121407(R) (2010).
[33] R. Bistritzer and A. H. MacDonald, Moire bands in twisted double-layer graphene, Proceedings of the National Academy

of Sciences **108**, 12233 (2011).
[34] Y. Cao, V. Fatemi, S. Fang, K. Watanabe, T. Taniguchi, E. Kaxiras, and P. Jarillo-Herrero, Unconventional superconductivity in magic-angle graphene superlattices, Nature **556**, 43 (2018).
[35] Y. Cao, V. Fatemi, A. Demir, S. Fang, S. L. Tomarken, J. Y. Luo, J. D. Sanchez-Yamagishi, K. Watanabe, T. Taniguchi, E. Kaxiras, R. C. Ashoori, and P. Jarillo-Herrero, Correlated insulator behaviour at half-filling in magic-angle graphene superlattices, Nature **556**, 80 (2018).
[36] M. Yankowitz, S. Chen, H. Polshyn, Y. Zhang, K. Watanabe, T. Taniguchi, D. Graf, A. F. Young, and C. R. Dean, Tuning superconductivity in twisted bilayer graphene, Science **363**, 1059 (2019).
[37] X. Lu, P. Stepanov, W. Yang, M. Xie, M. A. Aamir, I. Das, C. Urgell, K. Watanabe, T. Taniguchi, G. Zhang, A. Bachtold, A. H. MacDonald, and D. K. Efetov, Superconductors, orbital magnets and correlated states in magic-angle bilayer graphene, Nature **574**, 653 (2019).
[38] E. Y. Andrei and A. H. MacDonald, Graphene bilayers with a twist, Nature Materials **19**, 1265 (2020).
[39] V. L. Berezinskiĭ, Destruction of Long-range Order in One-dimensional and Two-dimensional Systems having a Continuous Symmetry Group I. Classical Systems, Soviet Journal of Experimental and Theoretical Physics **32**, 493 (1971).
[40] J. M. Kosterlitz and D. J. Thouless, Ordering, metastability and phase transitions in two-dimensional systems, Journal of Physics C: Solid State Physics **6**, 1181 (1973).
[41] K. Yang, K. Moon, L. Zheng, A. H. MacDonald, S. M. Girvin, D. Yoshioka, and S.-C. Zhang, Quantum ferromagnetism and phase transitions in double-layer quantum hall systems, Phys. Rev. Lett. **72**, 732 (1994).
[42] K. Moon, H. Mori, K. Yang, S. M. Girvin, A. H. MacDonald, L. Zheng, D. Yoshioka, and S.-C. Zhang, Spontaneous interlayer coherence in double-layer quantum hall systems: Charged vortices and kosterlitz-thouless phase transitions, Phys. Rev. B **51**, 5138 (1995).
[43] Supplementary material, which includes Refs. [13, 33, 42, 44–46, 48, 49, 51, 62–65]
[44] J. Jung, A. Raoux, Z. Qiao, and A. H. MacDonald, Ab initio theory of moiré superlattice bands in layered two-dimensional materials, Phys. Rev. B **89**, 205414 (2014).
[45] S. Carr, S. Fang, P. Jarillo-Herrero, and E. Kaxiras, Pressure dependence of the magic twist angle in graphene superlattices, Physical Review B **98**, 085144 (2018).
[46] M. Xie and A. H. Macdonald, Nature of the Correlated Insulator States in Twisted Bilayer Graphene, Physical Review Letters **124**, 097601 (2020).
[47] T. J. Peltonen, R. Ojajärvi, and T. T. Heikkilä, Mean-field theory for superconductivity in twisted bilayer graphene, Phys. Rev. B **98**, 220504(R) (2018).
[48] F. Wu, A. H. MacDonald, and I. Martin, Theory of Phonon-Mediated Superconductivity in Twisted Bilayer Graphene, Physical Review Letters **121**, 257001 (2018).
[49] T. Löthman and A. M. Black-Schaffer, Universal phase diagrams with superconducting domes for electronic flat bands, Phys. Rev. B **96**, 064505 (2017).
[50] N. Bultinck, S. Chatterjee, and M. P. Zaletel, Mechanism for Anomalous Hall Ferromagnetism in Twisted Bilayer Graphene, Phys. Rev. Lett. **124**, 166601 (2020).
[51] R. Ojajärvi, T. Hyart, M. A. Silaev, and T. T. Heikkilä, Competition of electron-phonon mediated superconductivity and Stoner magnetism on a flat band, Phys. Rev. B **98**, 054515 (2018).
[52] X. Hu, T. Hyart, D. I. Pikulin, and E. Rossi, Geometric and conventional contribution to the superfluid weight in twisted bilayer graphene, Phys. Rev. Lett. **123**, 237002 (2019).
[53] S. Peotta and P. Törmä, Superfluidity in topologically nontrivial flat bands, Nature Communications **6**, 8944 (2015).
[54] L. Liang, T. I. Vanhala, S. Peotta, T. Siro, A. Harju, and P. Törmä, Band geometry, Berry curvature, and superfluid weight, Phys. Rev. B **95**, 024515 (2017).
[55] F. Xie, Z. Song, B. Lian, and B. A. Bernevig, Topology-bounded superfluid weight in twisted bilayer graphene, Phys. Rev. Lett. **124**, 167002 (2020).
[56] A. Julku, T. J. Peltonen, L. Liang, T. T. Heikkilä, and P. Törmä, Superfluid weight and Berezinskii-Kosterlitz-Thouless transition temperature of twisted bilayer graphene, Phys. Rev. B **101**, 060505(R) (2020).
[57] J. Cao, H. A. Fertig, and L. Brey, Quantum geometric exciton drift velocity, Phys. Rev. B **103**, 115422 (2021).
[58] Q. Shi, E.-M. Shih, D. Rhodes, B. Kim, K. Barmak, K. Watanabe, T. Taniguchi, Z. Papi, D. A. Abanin, J. Hone, and C. R. Dean, Bilayer wse_2 as a natural platform for interlayer exciton condensates in the strong coupling limit (2021), arXiv:2108.10477 [cond-mat.mes-hall].
[59] J. Jang, H. M. Yoo, L. N. Pfeiffer, K. W. West, K. W. Baldwin, and R. C. Ashoori, Strong interlayer charge transfer due to exciton condensation in an electrically isolated gaas quantum well bilayer, Applied Physics Letters **118**, 202110 (2021).
[60] Z. Zhang, E. C. Regan, D. Wang, W. Zhao, S. Wang, M. Sayyad, K. Yumigeta, K. Watanabe, T. Taniguchi, S. Tongay, M. Crommie, A. Zettl, M. P. Zaletel, and F. Wang, Correlated interlayer exciton insulator in double layers of monolayer wse2 and moiré ws2/wse2 (2021), arXiv:2108.07131 [cond-mat.mes-hall].
[61] J. Towns, T. Cockerill, M. Dahan, I. Foster, K. Gaither, A. Grimshaw, V. Hazlewood, S. Lathrop, D. Lifka, G. D. Peterson, R. Roskies, J. R. Scott, and N. Wilkins-Diehr, Xsede: Accelerating scientific discovery, Computing in Science & Engineering **16**, 62 (2014).
[62] A. Lau, T. Hyart, C. Autieri, A. Chen, and D. I. Pikulin, Designing three-dimensional flat bands in nodal-line semimetals, Phys. Rev. X **11**, 031017 (2021).
[63] R. Côté, L. Brey, and A. H. MacDonald, Broken-symmetry ground states for the two-dimensional electron gas in a double-quantum-well system, Phys. Rev. B **46**, 10239 (1992).
[64] X.-W. Luo and C. Zhang, Spin-twisted optical lattices: Tunable flat bands and larkin-ovchinnikov superfluids, Phys. Rev. Lett. **126**, 103201 (2021).
[65] H. J. Monkhorst and J. D. Pack, Special points for brillouin-zone integrations, Phys. Rev. B **13**, 5188 (1976).